Front. Chem. Sci. Eng. 2021, 15(1): 99–108
https://doi.org/10.1007/s11705-020-1947-4

RESEARCH ARTICLE

Photocatalytic syngas synthesis from CO_2 and H_2O using ultrafine CeO_2-decorated layered double hydroxide nanosheets under visible-light up to 600 nm

Ling Tan*, Kipkorir Peter*, Jing Ren, Baoyang Du, Xiaojie Hao, Yufei Zhao (✉), Yu-Fei Song (✉)

State Key Laboratory of Chemical Resource Engineering, Beijing University of Chemical Technology, Beijing 100029, China

© Higher Education Press 2020

Abstract The rational design of photocatalyst that can effectively reduce CO_2 under visible light ($\lambda > 400$ nm), and simultaneously precise control of the products syngas (CO/H_2) ratio is highly desirable for the Fischer-Tropsch reaction. In this work, we synthesized a series of CeO_2-decorated layered double hydroxides (LDHs, Ce-*x*) samples for photocatalytic CO_2 reduction. It was found that the selectivity and productivity of CO and H_2 from photoreduction of CO_2 in conjunction with Ru-complex as photosensitizer performed an obvious "volcano-like" trend, with the highest point at Ce-0.15 and the CO/H_2 ratio can be widely tunable from 1/7.7 to 1/1.3. Furthermore, compared with LDH, Ce-0.15 also drove photocatalytic CO_2 to syngas under 600 nm irradiation. It implied that an optimum amount of CeO_2 modifying LDH promoted the photoreduction of CO_2 to syngas. This report gives the way to fully utilize the rare earth elements and provides a promising route to enhance the photo-response ability and charge injection efficiency of LDH-based photocatalysts in the synthesis of syngas with a tunable ratio under visible light irradiation.

Keywords visible light catalysis, CO_2 conversion, layered double hydroxide, rare earth elements

1 Introduction

Syngas (CO, H_2) with different ratio (1:1 to 1:3), as the main raw in C1 chemistry, plays a vital role in the synthesis of hydrocarbons, alcohols or fine chemicals through Fischer-Tropsch process, etc. In industry, the desirable ratio of syngas generally was produced from gasification of fossil fuels combination with water gas shift reaction ($CO + H_2O = CO_2 + H_2$) under harsh conditions, forming abundant of CO_2 as by-product. Photocatalysis provide an alternative and green approach for replacing the conventional thermal catalysis, mainly ascribe to the abundance of solar energy on Earth and the high selectivity to desirable products under mild reaction conditions. Photocatalyst for photoreduction of CO_2 (CO_2PR) into syngas in water with precise control of selectivity have attracted various attention for the utilization of renewable and clean energy [1–3]. In the past decades, various typical photocatalysts have been reported for efficient CO_2PR to syngas, such as C_3N_4 [4–6], TiO_2 [7–10], CeO_2 [11–13], $CuInS_x$ [2], CdS [14] etc., ascribed to their stability and environmental benignity. Although the performance of them have been fully investigated in the synthesis of CO from CO_2PR, the efficiency of CO_2PR still suffers from the weak absorption in the visible light region and relatively poor charge transfer in photocatalytic process, which has restricted those photocatalysts further industry application [15–17]. Therefore, achieving cost-effective catalysts with high performance in syngas synthesis, wider light absorption area and superior stability for CO_2PR remains a big challenge.

Amongst the reported photocatalysts, layered double hydroxides (LDHs) represent a typical inorganic two-dimensional (2D) materials with a formula $[M_{1-x}^{2+}M_x^{3+}(OH)_2]^{x+}(A^{n-})_{x/n}\cdot mH_2O$, where M^{2+} is the divalent cation, M^{3+} is trivalent cation in the laminate layers and A^{n-} is the interlaminated anion [18–23]. Owing to the special lamellar structure with highly dispersed metal elements and remarkable tunable light absorption capacity, LDHs are regarded as a promising photocatalysts for H_2O splitting [24], CO_2 reduction [25–29], N_2 fixation [30] and selective oxidation of benzene to phenol, etc [31–33]. Recently, several strategies (e.g., tuning the composition of

Received January 1, 2020; accepted April 10, 2020

E-mails: zhaoyufei@mail.buct.edu.cn (Zhao Y);
songyf@mail.buct.edu.cn (Song Y-F)

*These authors contributed equally to this work.

the LDHs host layers [34], loading Pd on the surface of LDHs [35–37], integrating with traditional catalysts (e.g., g-C_3N_4/NiAl-LDH and CoAl-LDH@TiO_2-NT) [25,26], intercalation [38], and defects engineering [39,40]) have been investigated to enhance the performance of LDHs-based photocatalysts. Nevertheless, due to poor charge mobility, serious recombination of photoinduced charge carriers is inevitable for traditional LDHs-based photocatalysts. Therefore, efforts for the efficient separation of photo-induced carriers and thus facilitating the interfacial kinetics are highly necessary for LDHs-based photocatalysts.

Cerium as one of typical rare earth elements (REEs) has been widely used for the catalytic conversion of automobile gasoline engine exhausts, CO oxidation, and some photocatalytic reactions, as mainly due to the abundance of oxygen vacancies with related to the easily passing from Ce^{3+} and Ce^{4+} [41–43]. Heterostructured photocatalysts that composing with two semiconductors could facilitate charge transfer, providing a promising strategy for the improvement of photocatalytic performance (e.g., Pd/Au/CeO_2 [44], Au/CeO_2 [45]). Compared with pristine CeO_2, the heterostructured CeO_2 structure exhibits superior performance in CO_2PR under visible light irradiation by narrowing the bandgap of CeO_2 [46,47]. Therefore, heterostructured photocatalysts designed reasonably have considerable prospects for the efficient CO_2PR for syngas synthesis.

Herein, a series of heterostructured CeO_2/LDHs with different loading of CeO_2 (denoted as, Ce-x, x = 0.05, 0.10, 0.15, 0.20, 0.30 and 0.40) were prepared via hydrothermal method. The selectivity and productivity of product syngas (CO and H_2) in CO_2PR under visible light performed a distinct "volcano-like" trend in conjunction with Ru-complex photosensitizer, with the tunable CO/H_2 ratio from 1/7.7 to 1/1.3 and the highest CO evolution rate of 85 $\mu mol \cdot g^{-1} \cdot h^{-1}$ at Ce-0.15 photocatalysts. Compared with pristine LDH, the Ce-0.15 photocatalyst displayed moderate photo-induced charge separation/transformation efficiency as confirmed by photoluminescence and electrochemical measurements. Furthermore, the Ce-0.15 can even drive CO_2PR to syngas under 600 nm irradiation. In all, this work reports a sustainable route for the synthesis of syngas with tunable ratio using heterostructured CeO_2/LDHs photocatalysts under visible light irradiation (Scheme 1).

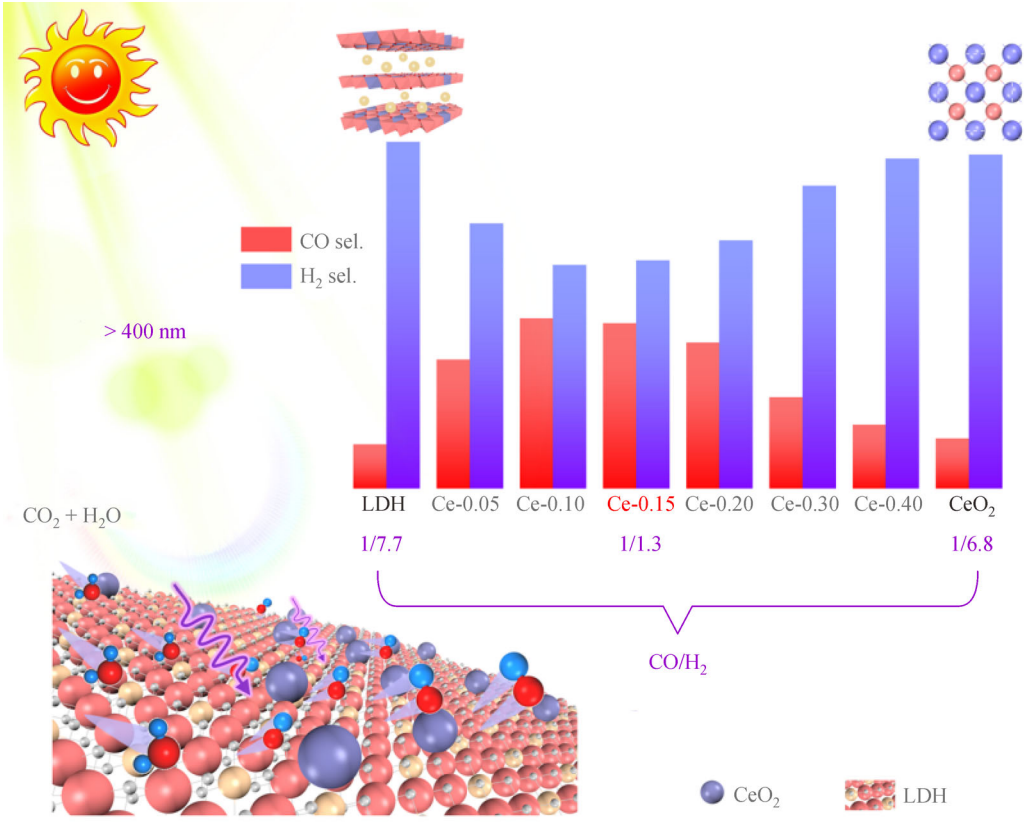

Scheme 1 Scheme of the tunable selectivity of syngas from photocatalytic CO_2 reduction by LDH, Ce-x (x = 0.05, 0.10, 0.15, 0.20, 0.30 and 0.40) and CeO_2 in conjunction with Ru-complex photosensitizer.

2 Experimental

2.1 Materials

$AlCl_3 \cdot 6H_2O$, $CeCl_3 \cdot 6H_2O$, $MgCl_2 \cdot 6H_2O$, KOH, and KCl, Na_2SO_4, $Ru(bpy)_3Cl_2 \cdot 6H_2O$, triethanolamine (TEOA) and acetonitrile were purchased from Sigma-Aldrich Co. and used directly without any purification. Pure CO_2 gas (99.999%) was purchased from Beijing Beiwen Gas Co. and used directly as a substrate for photocatalytic reduction. The water used in the synthesis of the materials was deionized.

2.2 Methods

2.2.1 Synthesis of CeO_2 modified $Mg_6Al_{2-x}Ce_x$-LDH (denoted as Ce-*x*)

A series of CeO_2 modified MgAl-LDH were prepared by the hydrothermal method using chloride salts of Mg, Al and Ce where $0 \leqslant x \leqslant 0.40$ [48]. Typically, aqueous solutions containing $MgCl_2 \cdot 6H_2O$, $AlCl_3 \cdot 6H_2O$ and $CeCl_3 \cdot 6H_2O$ in the ratios of (i) 24:8:0, (ii) 24:7.8:0.2, (iii) 24:1.6:0.40, (iv) 24:7.4:0.6, (v) 24:7.2:0.8, (vi) 24:6.8:1.2 and (vii) 24:6.4:1.6 together with 5.899 g of KCl were prepared in 80 mL of deionized H_2O. The mixed solution was vigorously stirred about 10 min and then adjusted to pH = 10 with drop-wise addition of 2 $mol \cdot L^{-1}$ KOH solution. The slurry was further stirred for 20 min, then transferred to 100 mL Teflon-lined stainless steel autoclave, and treated at 65 °C about 18 h. The resulting milky white to pale yellow product was centrifuged and washed to pH = 7. The product was oven-dried at 50 °C about 12 h.

2.2.2 Characterization

X-ray diffraction (XRD) patterns were characterized from Rigaku XRD. Infrared measurements were examined by Bruker 22 Fourier transform infrared spectroscopy equipment. Scanning electron microscopy (SEM) images were obtained on Zeiss Supra 55 SEM. High-resolution transmission electron microscopy (HRTEM) images were recorded on a JEOL JEM-2010. Brunauer-Emmett-Teller (BET) surface area was obtained on Quantachrome Autosorb-1C analyzer. UV-visible spectra were collected on a Beijing PGENERAL TU-1901. X-ray photoelectron spectroscopy (XPS) spectra were calibrated against C 1s (284.8 eV). The photoluminescence (PL) spectra were collected on Shimadzu RF-6000 at room temperature.

Electrochemical impedance spectroscopy (EIS) spectra were performed on CHI760A electrochemical workstation (Shanghai Chenhua, China). The Ce-*x* modified glassy carbon electrode was employed as a working electrode, Pt electrode was regarded as counter electrode and saturated calomel electrode was used as reference electrode. 1 cm^2 area of glassy carbon electrodes, 130 μL of homogeneous Nafion-treated Ce-*x* sample suspension was applied. The sample suspension was dispersed by adding 50 μL of Nafion and 2 mg of Ce-*x* in 1 mL ethanol.

2.2.3 Photocatalytic CO_2 reduction

Photocatalytic CO_2 reduction was explored in a 50 mL closed stainless reactor. At first, 10 mg Ce-*x* was dispersed in the 10 mL solution (H_2O:CH_3CN:TEOA = 1:3:1 (v:v:v)), next 3.3 mg $[Ru(bpy)_3]Cl_2 \cdot 6H_2O$ was added into the mixed system, and then the reactor was evaculated and refilled with pure CO_2. Finally, 0.18 MPa CO_2 was filled into the reactor. The performance of each photocatalyst was checked at 30 °C with 300 W Xe lamp under visible light. The products were analyzed by Shimadzu GC-2014 chromatography with flame ionization detector and thermal conductivity detector. The isotopic experiment was carried out under the same condition filling $^{13}CO_2$ (Linde Gas Comp. 99%) using gas chromatography-mass spectrometry (GC-MS, QP2020) to check the products.

3 Results and discussion

MgAl-LDH was chosen as support for loading CeO_2, since MgAl-LDH was one of the most successful scale-up LDH based products in the industry due to the easy synthesis and cheap raw materials. A series of Ce-*x* samples were prepared by co-precipitation method and followed by hydrothermal treatment, as the previous report [48]. As presented in Fig. 1, the peaks of (00*l*), (110) and (113) in XRD patterns and the weakness carbonate feature at 1373 cm^{-1} in the FTIR spectra illustrated the successful synthesis of CO_3^{2-} intercalated LDH structure. The modified Ce did not affect the crystal structure of LDHs. More interestingly, the intensity of peak at 28° in XRD patterns ascribed to (111) of CeO_2 in cubic fluorite structure [12,47,49], enhanced with increasing the amount of Ce in LDHs structure. Furthermore, the Ce-*x* structure possessed type IV isotherm adsorption curves and BET surface area of Ce-0.15 was 116.9 $m^2 \cdot g^{-1}$, which was highest among the as-prepared catalyst (Fig. 1(c) and Table S1 (cf. Electronic Supplementary Material, ESM), demonstrated that Ce-0.15 provided the larger reaction area and more active sites for the photocatalysis. Ce-0.15 also exhibited relatively uniform mesopores with a narrow pore diameter distribution (4–9 nm) (Fig. 1(d)), thus may benifical for the diffusion of reactants, playing a key role in the following photocatalytic efficiency [43], as discussed below.

The SEM (Fig. S1, cf. ESM) and TEM (Fig. 2) images showed nanosheet morphology of LDHs-based substrate. Besides, there were some black dots on the LDHs

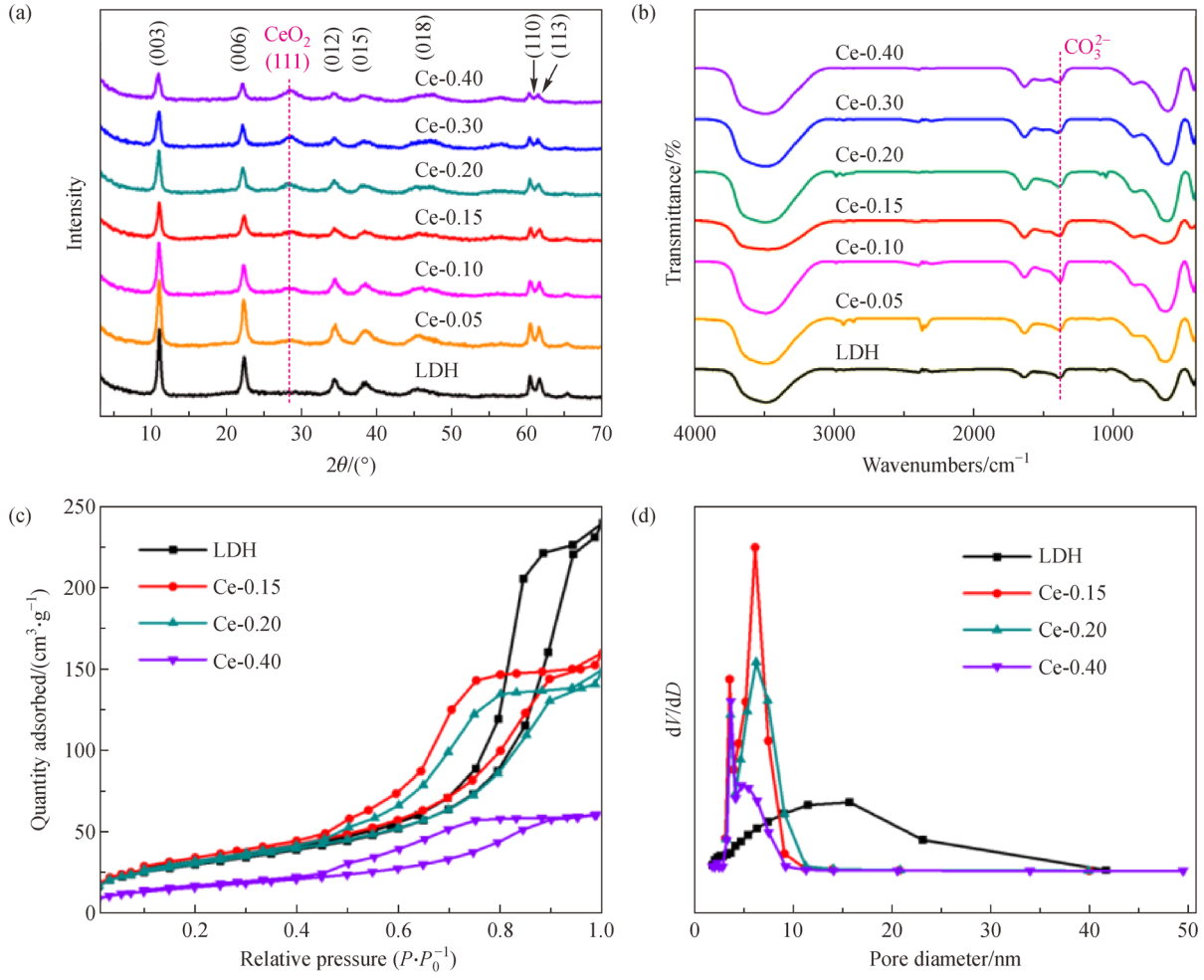

Fig. 1 (a) XRD patterns and (b) FTIR spectra of LDH and Ce-*x* (*x* = 0.05, 0.10, 0.15, 0.20, 0.30 and 0.40), respectively; (c) BET of the as-synthesized LDH, Ce-*x* (*x* = 0.15, 0.20 and 0.40) and (d) the corresponding pore size distribution.

nanosheet, which was corresponding to the CeO_2 nanostructure. The size of ultrathin CeO_2 nanoparticles was determined to be ~3.19 nm (Fig. 2(c) inset). Meanwhile, as presented in HRTEM images (Fig. 2(d)), a lattice fringe spacing of 0.30 nm can be determined to be the (111) facet of CeO_2 [11]. Moreover, the energy-dispersive X-ray spectroscopy mapping images suggested the uniform distributions of Mg, Al, O and Ce over the entire Ce-0.15 structure (Fig. S2, cf. ESM). Furthermore, the ratio of Mg/Al/Ce in LDH and Ce-*x* (*x* = 0.05, 0.10, 0.15, 0.20, 0.30 and 0.40) was measured to be 3.64:1.00:0.00, 3.62:1.00:0.01, 3.63:1.00:0.03, 3.60:1.00:0.06, 3.66:1.00:0.09, 3.68:1.00:0.19 and 3.65:1.00:0.59, respectively, as presented in Fig. S2(f) and Fig. S3 (cf. ESM). It proved that the intensity of CeO_2 concentration was enhanced with increasing the amount of Ce in the synthetic process. The surface characteristics and chemical compositions of Ce-*x* were determined via XPS measurement (Fig. S4, cf. ESM). As shown in Fig. S4(a), the XPS spectra provided complete views of the surface elemental compositions of Ce-*x*, which all showed the presence of Mg and Al elements. With increasing the Cerium concentration, the enhanced intensity of Ce 3d and the presence of Ce^{4+} in Ce-*x* can be ascribed to the modified CeO_2 in LDHs nanosheets. Besides, the Mg 1s, Al 2p or O 1s exhibited similar to each other in Ce-*x*, indicating the modified of CeO_2 had little effect on the structure of LDHs.

The photocatalytic activity of as-prepared photocatalysts (Ce-*x*) was investigated under visible light in conjunction with Ru-complex and TEOA served as a photosensitizer and sacrificial agent in CO_2 atmosphere as previous reports [50,51]. Based on the ^{1}H-NMR result (Figure S5), no detectable liquid chemicals such as HCHO, CH_3OH and HCOOH were formed. As shown in Fig. 3(a), LDH, Ce-*x* and also CeO_2 gave the only products of syngas (CO and H_2), in detail, the selectivity of CO gave 11.4% for LDH, through decorating CeO_2 on the surface of LDH, the CO selectivity further increased to 42.1% for Ce-0.15, and

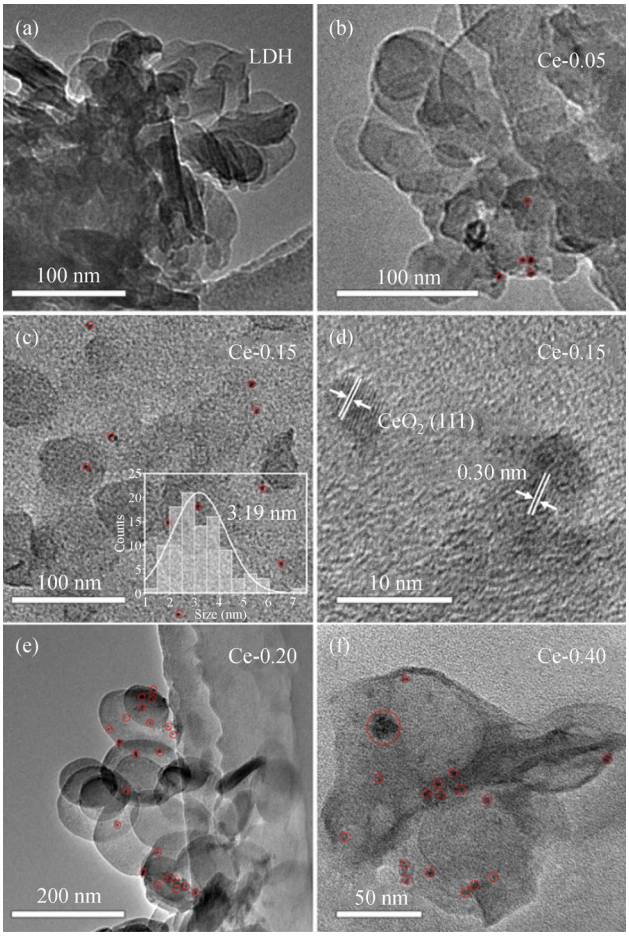

Fig. 2 TEM images of (a) LDH, (b) Ce-0.05, (c) Ce-0.15, and the corresponding particle size distribution of CeO_2 (the insert picture of Fig. 2(c)), (d) HRTEM image of Ce-0.15; TEM images of (e) Ce-0.20 and (f) Ce-0.40.

further increasing the loading amount of CeO_2, the CO selectivity decreased to 16.4% (Ce-0.40), nearly the same as that of referenced CeO_2 (12.9%). The ratio of syngas (CO/H_2) can be optimized from 1/7.1 (LDH) to 1/1.30 (Ce-0.15) with the highest CO selectivity of 42.1% for Ce-0.15. This tunable syngas is much beneficial for the methanol synthesis and Fischer-Tropsch process in the industry. As shown in Fig. 3(b), the productivity of CO can be also optimized to 0.85 μmol (Ce-0.15), 4.7 and 9.4 times higher than that of LDH (0.18 μmol) and CeO_2 (0.09 μmol), respectively. In all, the selectivity and productivity trend of CO performed an obvious "volcano-like" trend, with the highest point at Ce-0.15 (42.1% selectivity to CO with a rate of 85 $\mu mol \cdot g^{-1} \cdot h^{-1}$). The reason for Ce-0.15 performed outstanding selectivity and activity in CO_2PR will be further discussed.

Furthermore, GC-MS was employed to verify the origin of as-produced CO. As shown in Fig. 3(c), the $^{12}CO_2$ or $^{13}CO_2$ was used as a reactant and the corresponding signal of ^{12}CO or ^{13}CO was m/z = 28 or 29, respectively, indicating the produced CO originated from the photoreduction of CO_2 gas source (Fig. 3(c)). As shown in Fig. 3(d) and Fig. S6 (cf. ESM), ultrahigh selectivity of H_2 in Ar atmosphere (100%, 0.01 μmol) or without adding Ce-0.15 (97.1%, 1.53 μmol) in CO_2PR and no detectable products were generated without adding $Ru(bpy)_3Cl_2$ and in dark experimental condition. These control experiments indicated the $Ru(bpy)_3Cl_2$ together with Ce-x played an important role in CO_2PR. In addition, the Ce-0.15 photocatalyst can be recycled at least four times, the selectivity (Fig. 3(e)) and productivity (Fig. 3(f)) nearly maintained as the first cycle, proving the stability of the as-synthesized photocatalyst. The XRD pattern (Fig. S7) and TEM images (Fig. S8, cf. ESM) of recycled Ce-0.15 also proved its good stability.

The UV-vis spectra of Ce-x were collected to gauge their light absorption ability to explore the influence factor of their photocatalytic activity. As shown in Fig. 4(a), CeO_2 showed two absorption peaks at 280 and 320 nm, which was attributed to the absorption of Ce^{3+} and Ce^{4+}, respectively [43]. The MgAl-LDH only absorbed UV light and the absorbance range was improved to a visible light area with modifying CeO_2 on the surface of LDH. Most interestingly, the Ce-0.15 photocatalyst exhibited the highest absorbance intensity in the visible range, which may be ascribed to the optimal interaction effect between CeO_2 and LDH [47]. Accordingly, we investigated the performance of Ce-0.15 and LDH in CO_2PR under different cut-off filter light irradiation (Fig. S9, cf. ESM) to reveal the effect of CeO_2 modification on LDH, especially with the presence of photosensitizer $Ru(bpy)_3Cl_2 \cdot 6H_2O$ since its much wider visible light absorbance from ~600 to 200 nm (Fig. 4(b)). As shown in Figs. 4(c,d) and Fig. S10 (cf. ESM), the performance of both LDH and CeO_2 decreased with increasing the irradiation wavelength from 405 to 600 nm, and LDH did not exhibit any photoactivity under irradiation 600 nm, mainly due to the limited light absorbance ability. Especially, under 600 nm irradiation, we found the productivity/selectivity of CO was 0.05 μmol, 8.7% and the productivity/selectivity of H_2 was 0.52 μmol, 91.3% by Ce-0.15, respectively. The external quantum efficiency of CO still retain 0.05% (Ce-0.15) under irradiation at 600 nm (Table S2) compared with 0% of LDH. From previous reports (Table S3, cf. ESM), Ce-x achieved precise control of the products syngas (CO/H_2) ratio under > 400 nm and were able to convert CO_2 to syngas under 600 nm irradiation, this 600 nm induced syngas synthesis from CO_2 can be well understood due to the heterostructure CeO_2/LDH.

To reveal the optoelectronic properties and intrinsic reasons for the efficient syngas synthesis from CO_2PR on Ce-0.15, we investigated the PL and EIS spectra. As shown in PL spectra (Fig. 5(a)), a moderate weaker

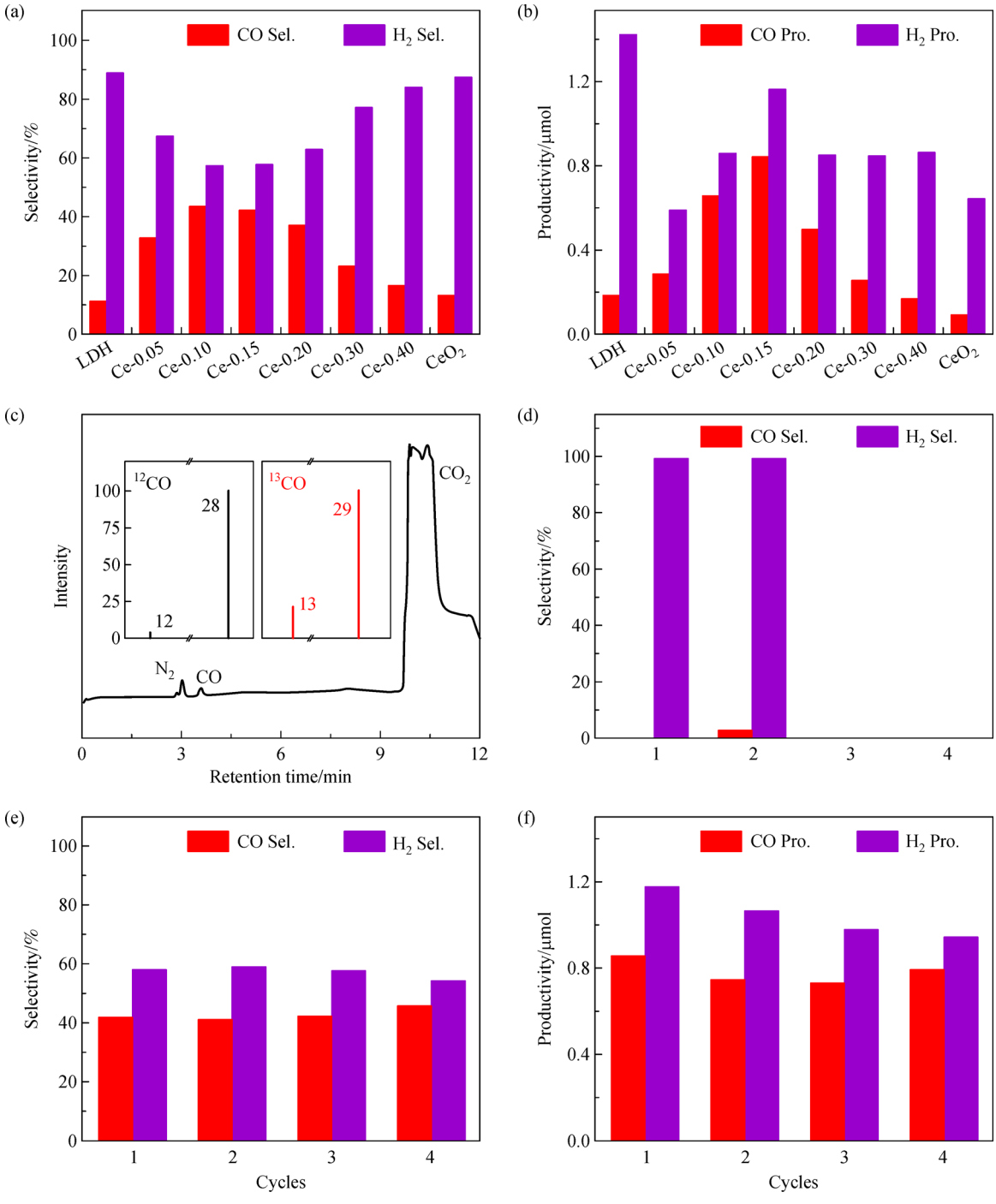

Fig. 3 The (a) selectivity, (b) productivity of LDH and Ce-x (x = 0.05, 0.10, 0.15, 0.20, 0.30 and 0.40, respectively) and CeO_2 in CO_2PR under visible light irradiation; (c) isotope trace analysis GC-MS spectra using Ce-0.15 photocatalysts; (d) the selectivity of catalyst under control experimental reaction conditions (1. Ar atmosphere; 2. Without Ce-0.15; 3. Without $Ru(bpy)_3Cl_2$; 4. In dark); (e) selectivity and (f) productivity of recycle Ce-0.15.

photoluminescence emission of $Ru(bpy)_3Cl_2$ on Ce-0.15 than other samples proved efficient electron-hole separation between Ce-0.15 and $Ru(bpy)_3Cl_2$ in photocatalysis. In addition, EIS spectra (Fig. 5(b)) confirmed that Ce-0.15 provided relative decreased charge transfer resistance comparing with pristine LDH, which further indicated the efficient separation and transfer of photogenerated electron-hole pairs. The improved conductivity of Ce-0.4 may be ascribed to the enhanced interaction between CeO_2 and LDH. Above all, a possible reaction mechanism was

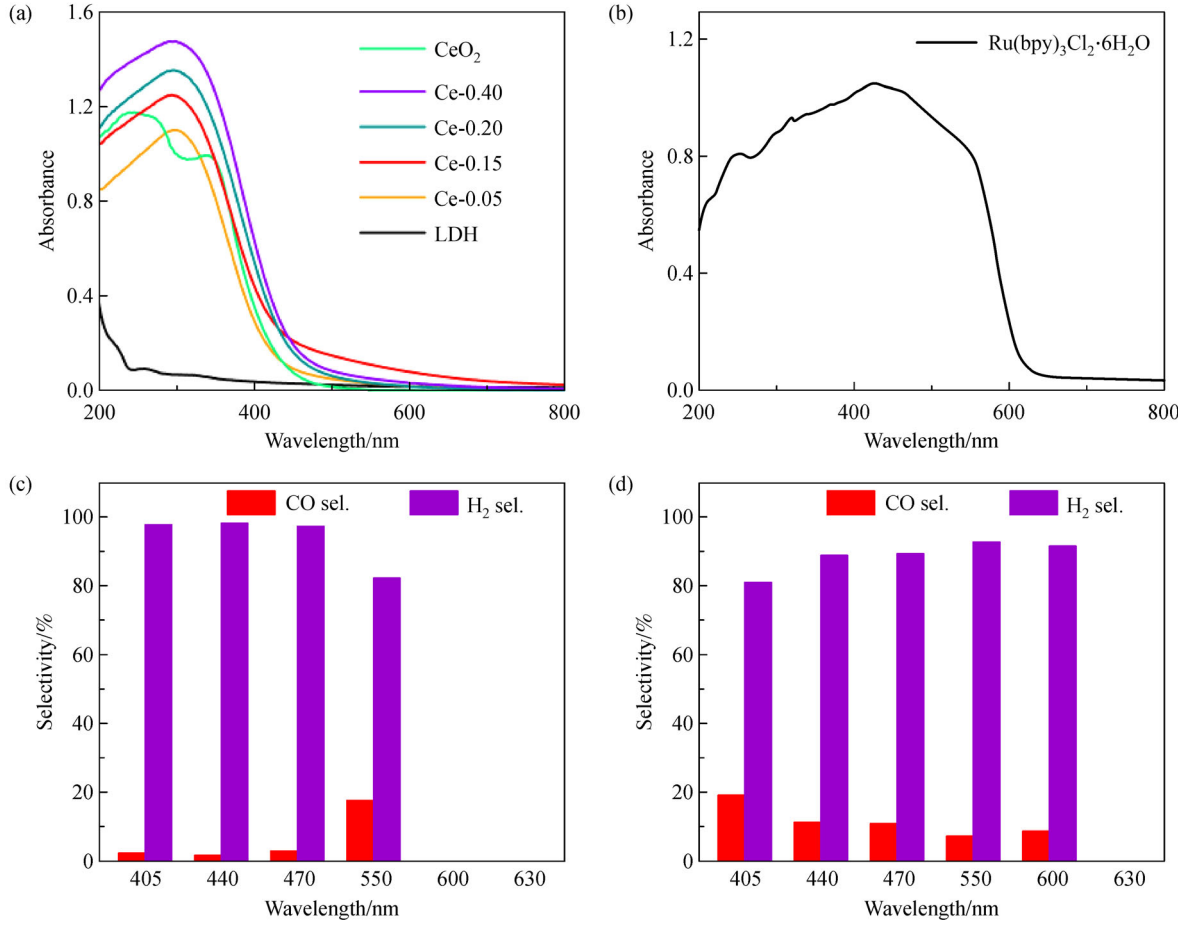

Fig. 4 The UV-vis spectra of (a) LDH, Ce-*x* and CeO_2, (b) the photosensitizer $Ru(bpy)_3Cl_2 \cdot 6H_2O$ as our previous report [39] and the selectivity of (c) LDH and (d) Ce-0.15 in CO_2PR under different cut-off filter light irradiation.

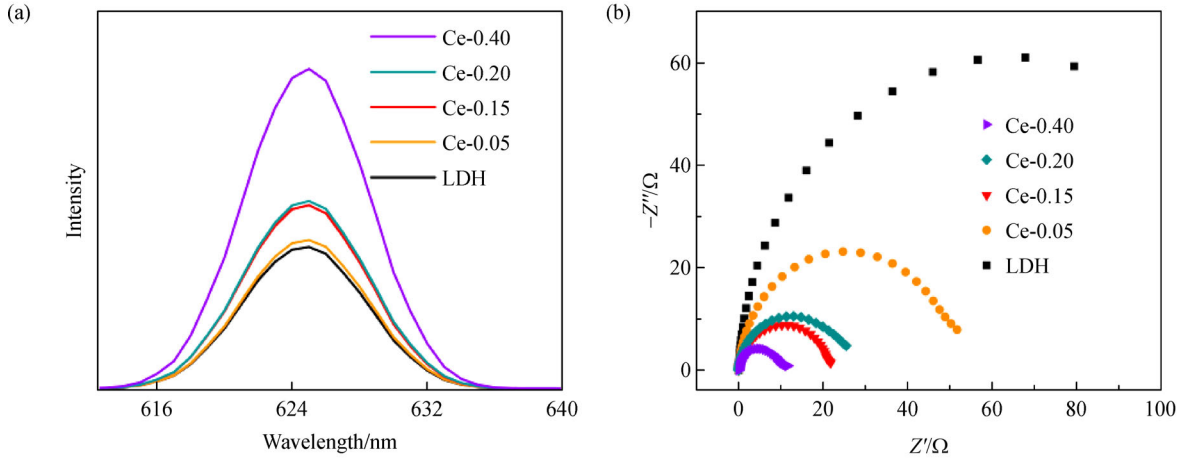

Fig. 5 (a) PL spectra of as-synthesized catalyst in a solution containing 4×10^{-6} mol $Ru(bpy)_3Cl_2 \cdot 6H_2O$; (b) EIS spectra of the as-synthesized LDH and Ce-*x*.

proposed as follows (Scheme S1, cf. ESM), under visible light irradiation, the Ru photosensitizer was activated to the excited state ($[Ru(bpy)_3]^{2+}$*) [50], and the photo-induced electrons from the excited state directly transferred to the surface of catalysts (LDH and CeO_2). Subsequently, the electrons produced the reduction reaction (splitting water into active hydrogen species (H*)) [40,52], then the absorbed CO_2 molecules on the surface of catalyst were further hydrogenated with 2 equivalence mol of active H* for the formation of CO; meantime, the surface-active H* can be easily coupling for the evolution of H_2. This competition between hydrogenation and coupling of surface-active H* resulted in the tunable selectivity of syngas (CO and H_2). Finally, the oxidized $[Ru(bpy)_3]^{3+}$ can be returned to $[Ru(bpy)_3]^{2+}$ with the assistance of sacrificial agent (TEOA) [37]. For the pure LDH and CeO_2 structure, the photoinduced H* on the surface preferred to coupling rather than hydrogenation, leading to the formation of much more favourable H_2 evolution rather than the valuable product CO, mainly due to the rapid electron-hole recombination. Desirably, for the hetero-structured CeO_2/LDH (Ce-0.15), moderate separation efficiency of electron-hole by suppressing their recombination, resulted in an enhanced hydrogenation reaction for the CO evolution around the abundant of interfaces in heterostructured CeO_2/LDH, explaining the enhanced CO_2PR to CO, and the tunable ratio of syngas.

4 Conclusions

In summary, a series of Ce-*x* samples were successfully synthesized by co-precipitation method and followed by hydrothermal treatment. We found that the selectivity and productivity of syngas performed an obvious "volcano-like" trend, with the highest point at Ce-0.15. And the ratio of the products of CO/H_2 (syngas) can be tunable from 1/7.1 (LDH) to 1/1.30 (Ce-0.15). More importantly, Ce-0.15 can drove CO_2PR to syngas under 600 nm irradiation. UV-vis, PL, and EIS revealed that Ce-0.15 performed a suitable separation and transfer of photogenerated electron-hole in photocatalysis. This work paves the way to fully utilize the rare earth elements and stimulates the development of REEs-based catalysts in the synthesis of syngas under solar irradiation. Other rare-earth element (like Er) doped LDH for photoreduction of CO_2 is underway in our lab.

Acknowledgements This research was supported by the National Natural Science Foundation of China (Grant Nos. U1707603, 21878008, 21625101, U1507102, 21922801), Beijing Natural Science Foundation (Nos. 2182047, 2202036) and the Fundamental Research Funds for the Central Universities (Nos. XK1802-6, XK1902, 12060093063, 2312018RC07).

Electronic Supplementary Material Supplementary material is available in the online version of this article at https://doi.org/10.1007/s11705-020-1947-4 and is accessible for authorized users.

References

1. Li X, Yu J, Jaroniec M, Chen X. Cocatalysts for selective photoreduction of CO_2 into solar fuels. Chemical Reviews, 2019, 119(6): 3962–4179
2. Li X, Sun Y, Xu J, Shao Y, Wu J, Xu X, Pan Y, Ju H, Zhu J, Xie Y. Selective visible-light-driven photocatalytic CO_2 reduction to CH_4 mediated by atomically thin $CuIn_5S_8$ layers. Nature Energy, 2019, 4 (8): 690–699
3. Zhao Y, Waterhouse G I N, Chen G, Xiong X, Wu L Z, Tung C H, Zhang T. Two-dimensional-related catalytic materials for solar-driven conversion of CO_x into valuable chemical feedstocks. Chemical Society Reviews, 2019, 48(7): 1972–2010
4. Huang P P, Huang J H, Pantovich S A, Carl A D, Fenton T G, Caputo C A, Grimm R L, Frenkel A I, Li G H. Selective CO_2 reduction catalyzed by single cobalt sites on carbon nitride under visible-light irradiation. Journal of the American Chemical Society, 2018, 140(47): 16042–16047
5. Kuriki R, Yamamoto M, Higuchi K, Yamamoto Y, Akatsuka M, Lu D L, Yagi S, Yoshida T, Ishitani O, Maeda K. Robust binding between carbon nitride nanosheets and a binuclear ruthenium(II) complex enabling durable, selective CO_2 reduction under visible light in aqueous solution. Angewandte Chemie International Edition, 2017, 56(17): 4867–4871
6. Kuriki R, Sekizawa K, Ishitani O, Maeda K. Visible-light-driven CO_2 reduction with carbon nitride: Enhancing the activity of ruthenium catalysts. Angewandte Chemie International Edition, 2015, 54(8): 2406–2409
7. Lee J S, Won D I, Jung W J, Son H J, Pac C, Kang S O. Widely controllable syngas production by a dye-sensitized TiO_2 hybrid system with Re(I) and Co(III) catalysts under visible-light irradiation. Angewandte Chemie International Edition, 2017, 56 (4): 976–980
8. Won D I, Lee J S, Ji J M, Jung W J, Son H J, Pac C, Kang S O. Highly robust hybrid photocatalyst for carbon dioxide reduction: Tuning and optimization of catalytic activities of Dye/TiO_2/Re(I) organic-inorganic ternary systems. Journal of the American Chemical Society, 2015, 137(42): 13679–13690
9. Woolerton T W, Sheard S, Reisner E, Pierce E, Ragsdale S W, Armstrong F A. Efficient and clean photoreduction of CO_2 to CO by enzyme-modified TiO_2 nanoparticles using visible light. Journal of the American Chemical Society, 2010, 132(7): 2132–2133
10. Chen X, Liu L, Yu P Y, Mao S S. Increasing solar absorption for photocatalysis with black hydrogenated titanium dioxide nanocrystals. Science, 2011, 331(6018): 746–750
11. Li P, Zhou Y, Zhao Z, Xu Q, Wang X, Xiao M, Zou Z. Hexahedron prism-anchored octahedronal CeO_2: Crystal facet-based homojunction promoting efficient solar fuel synthesis. Journal of the American Chemical Society, 2015, 137(30): 9547–9550
12. Aneggi E, Wiater D, de Leitenburg C, Llorca J, Trovarelli A. Shape-dependent activity of ceria in soot combustion. ACS Catalysis, 2014, 4(1): 172–181
13. Tanaka A, Hashimoto K, Kominami H. Preparation of Au/CeO_2 exhibiting strong surface plasmon resonance effective for selective or chemoselective oxidation of alcohols to aldehydes or ketones in

aqueous suspensions under irradiation by green light. Journal of the American Chemical Society, 2012, 134(35): 14526–14533

14. Wang J, Xia T, Wang L, Zheng X, Qi Z, Gao C, Zhu J, Li Z, Xu H, Xiong Y. Enabling visible-light-driven selective CO_2 reduction by doping quantum dots: Trapping electrons and suppressing H_2 evolution. Angewandte Chemie International Edition, 2018, 57(50): 16447–16451
15. Ulmer U, Dingle T, Duchesne P N, Morris R H, Tavasoli A, Wood T, Ozin G A. Fundamentals and applications of photocatalytic CO_2 methanation. Nature Communications, 2019, 10(1): 3169
16. Bushuyev O S, De Luna P, Dinh C T, Tao L, Saur G, van de Lagemaat J, Kelley S O, Sargent E H. What should we make with CO_2 and how can we make it? Joule, 2018, 2(5): 825–832
17. Schultz D M, Yoon T P. Solar synthesis: Prospects in visible light photocatalysis. Science, 2014, 343(6174): 1239176
18. Yu J, Wang Q, O'Hare D, Sun L. Preparation of two dimensional layered double hydroxide nanosheets and their applications. Chemical Society Reviews, 2017, 46(19): 5950–5974
19. Yin H, Tang Z. Ultrathin two-dimensional layered metal hydroxides: An emerging platform for advanced catalysis, energy conversion and storage. Chemical Society Reviews, 2016, 45(18): 4873–4891
20. Fan G, Li F, Evans D G, Duan X. Catalytic applications of layered double hydroxides: Recent advances and perspectives. Chemical Society Reviews, 2014, 43(20): 7040–7066
21. Gao R, Yan D. Layered host-guest long-after glow ultrathin nanosheets: High-efficiency phosphorescence energy transfer at 2D confined interface. Chemical Science (Cambridge), 2017, 8(1): 590–599
22. Li T, Hao X, Bai S, Zhao Y, Song Y F. Controllable synthesis and scale-up production prospect of monolayer layered double hydroxide nanosheets. Acta Physico-chimica Sinica, 2020, 36: 1912005 (in Chinese)
23. Yin Q, Rao D, Zhang G, Zhao Y, Han J, Lin K, Zheng L, Zhang J, Zhou J, Wei M. CoFe-Cl layered double hydroxide: A new cathode material for high-performance chloride ion batteries. Advanced Functional Materials, 2019, 29(36): 1900983
24. Arif M, Yasin G, Shakeel M, Mushtaq M A, Ye W, Fang X, Ji S, Yan D. Hierarchical CoFe-layered double hydroxide and g-C_3N_4 heterostructures with enhanced bifunctional photo/electrocatalytic activity towards overall water splitting. Materials Chemistry Frontiers, 2019, 3(3): 520–531
25. Kumar S, Durndell L J, Manayil J C, Isaacs M A, Parlett C M A, Karthikeyan S, Douthwaite R E, Coulson B, Wilson K, Lee A F. Delaminated CoAl-layered double hydroxide@TiO_2 heterojunction nanocomposites for photocatalytic reduction of CO_2. Particle & Particle Systems Characterization, 2018, 35(1): 1700317
26. Tonda S, Kumar S, Bhardwaj M, Yadav P, Ogale S. g-C_3N_4/NiAl-LDH 2D/2D hybrid heterojunction for high-performance photocatalytic reduction of CO_2 into renewable fuels. ACS Applied Materials & Interfaces, 2018, 10(3): 2667–2678
27. Ahmed N, Shibata Y, Taniguchi T, Izumi Y. Photocatalytic conversion of carbon dioxide into methanol using zinc-copper-M (III) (M = aluminum, gallium) layered double hydroxides. Journal of Catalysis, 2011, 279(1): 123–135
28. Teramura K, Iguchi S, Mizuno Y, Shishido T, Tanaka T. Photocatalytic conversion of CO_2 in water over layered double hydroxides. Angewandte Chemie International Edition, 2012, 51 (32): 8008–8011
29. Izumi Y. Recent advances in the photocatalytic conversion of carbon dioxide to fuels with water and/or hydrogen using solar energy and beyond. Coordination Chemistry Reviews, 2013, 257 (1): 171–186
30. Arif M, Yasin G, Luo L, Ye W, Mushtaq M A, Fang X, Xiang X, Ji S, Yan D. Hierarchical hollow nanotubes of NiFeV-layered double hydroxides@CoVP heterostructures towards efficient, pH-universal electrocatalytical nitrogen reduction reaction to ammonia. Applied Catalysis B: Environmental, 2020, 265: 118559
31. Zhao Y, Jia X, Waterhouse G I N, Wu L Z, Tung C H, O'Hare D, Zhang T. Layered double hydroxide nanostructured photocatalysts for renewable energy production. Advanced Energy Materials, 2016, 6(6): 1501974
32. Li J, Xu Y, Ding Z, Mahadi A H, Zhao Y, Song Y F. Photocatalytic selective oxidation of benzene to phenol in water over layered double hydroxide: A thermodynamic and kinetic perspective. Chemical Engineering Journal, 2020, 388: 124248
33. Wang Q, Feng J, Zheng L, Wang B, Bi R, He Y, Liu H, Li D. Interfacial structure-determined reaction pathway and selectivity for 5-hydroxymethyl furfural hydrogenation over Cu-based catalysts. ACS Catalysis, 2020, 10(2): 1353–1365
34. Bai S, Wang Z, Tan L, Waterhouse G I N, Zhao Y, Song Y F. 600 nm irradiation-induced efficient photocatalytic CO_2 reduction by ultrathin layered double hydroxide nanosheets. Industrial & Engineering Chemistry Research, 2020, 59(13): 5848–5857
35. Silva C G, Bouizi Y, Forne's V, Garcia H. Layered double hydroxides as highly efficient photocatalysts for visible light oxygen generation from water. Journal of the American Chemical Society, 2009, 131(38): 13833–13839
36. Ren J, Ouyang S, Xu H, Meng X, Wang T, Wang D, Ye J. Targeting activation of CO_2 and H_2 over Ru-loaded ultrathin layered double hydroxides to achieve efficient photothermal CO_2 methanation in flow-type system. Advanced Energy Materials, 2017, 7(5): 1601657
37. Wang X, Wang Z, Bai Y, Tan L, Xu Y, Hao X, Wang J, Mahadi A H, Zhao Y, Zheng L, et al. Tuning the selectivity of photoreduction of CO_2 to syngas over Pd/layered double hydroxide nanosheets under visible-light up to 600 nm. Journal of Energy Chemistry, 2020, 46: 1–7
38. Kipkorir P, Tan L, Ren J, Zhao Y, Song Y F. Intercalation effect in NiAl-layered double hydroxide nanosheets for CO_2 reduction under visible light. Chemical Research in Chinese Universities, 2020, 36 (1): 127–133
39. Tan L, Xu S M, Wang Z, Xu Y, Wang X, Hao X, Bai S, Ning C, Wang Y, Zhang W, et al. Highly selective photoreduction of CO_2 with suppressing H_2 evolution over monolayer layered double hydroxide under irradiation above 600 nm. Angewandte Chemie International Edition, 2019, 58(34): 11860–11867
40. Hao X, Tan L, Xu Y, Wang Z, Wang X, Bai S, Ning C, Zhao J, Zhao Y, Song Y F. Engineering active Ni sites in ternary layered double hydroxides nanosheets for a high selectivity photoreduction of CO_2 to CH_4 under irradiation above 500 nm. Industrial & Engineering Chemistry Research, 2020, 59(7): 3008–3015

41. Montini T, Melchionna M, Monai M, Fornasiero P. Fundamentals and catalytic applications of CeO_2-based materials. Chemical Reviews, 2016, 116(10): 5987–6041
42. Li Y, He X, Yin J J, Ma Y, Zhang P, Li J, Ding Y, Zhang J, Zhao Y, Chai Z, Zhang Z. Acquired superoxide-scavenging ability of ceria nanoparticles. Angewandte Chemie International Edition, 2015, 54 (6): 1832–1835
43. Ye T, Huang W, Zeng L, Li M, Shi J. CeO_{2-x} platelet from monometallic cerium layered double hydroxides and its photocatalytic reduction of CO_2. Applied Catalysis B: Environmental, 2017, 210: 141–148
44. Zhang S, Chang C, Huang Z, Ma Y, Gao W, Li J, Qu Y. Visible-light-activated Suzuki-Miyaura coupling reactions of aryl chlorides over the multifunctional Pd/Au/porous nanorods of CeO_2 catalysts. ACS Catalysis, 2015, 5(11): 6481–6488
45. Primo A, Marino T, Corma A, Molinari R, Garcia H. Efficient visible-light photocatalytic water splitting by minute amounts of gold supported on nanoparticulate CeO_2 obtained by a biopolymer templating method. Journal of the American Chemical Society, 2011, 133(18): 6930–6933
46. Seftel E M, Puscasu M C, Mertens M, Cool P, Carja G. Assemblies of nanoparticles of CeO_2-ZnTi-LDHs and their derived mixed oxides as novel photocatalytic systems for phenol degradation. Applied Catalysis B: Environmental, 2014, 150-151: 157–166
47. Valente J S, Tzompantzi F, Prince J. Highly efficient photocatalytic elimination of phenol and chlorinated phenols by CeO_2/MgAl layered double hydroxides. Applied Catalysis B: Environmental, 2011, 102(1-2): 276–285
48. Iqbal K, Iqbal A, Kirillov A M, Wang B, Liu W, Tang Y. A new Ce-doped MgAl-LDH@Au nanocatalyst for highly efficient reductive degradation of organic contaminants. Journal of Materials Chemistry. A, Materials for Energy and Sustainability, 2017, 5(14): 6716–6724
49. Chen Y, Lv S, Chen C, Qiu C, Fan X, Wang Z. Controllable synthesis of ceria nanoparticles with uniform reactive {100} exposure planes. Journal of Chemical Physics, 2014, 118(8): 4437–4443
50. Gao C, Chen S, Wang Y, Wang J, Zheng X, Zhu J, Song L, Zhang W, Xiong Y. Heterogeneous single-atom catalyst for visible-light-driven high-turnover CO_2 reduction: The role of electron transfer. Advanced Materials, 2018, 30(13): 1704624
51. Rao H, Schmidt L C, Bonin J, Robert M. Visible-light-driven methane formation from CO_2 with a molecular iron catalyst. Nature, 2017, 548(7665): 74–77
52. Han B, Ou X, Deng Z, Song Y, Tian C, Deng H, Xu Y J, Lin Z. Nickel metal-organic frameworks monolayers for photoreduction of diluted CO_2: Metal-node-dependent activity and selectivity. Angewandte Chemie International Edition, 2018, 57(51): 16811–16815